Crystal Structure Theory and Applications, 2026, 14(1), 1-13
https://www.scirp.org/journal/csta
ISSN Online: 2169-2505
ISSN Print: 2169-2491

Structural and Electronic Properties of $Zn_{1-x}Mg_xO$ Alloys in WZ Phase with Hubbard Correction: Prospective Material for Optoelectronics Applications

Ismaïla S. Badji*, Alassane Diaw, Moulaye Diagne, Modou Pilor, Nacire Mbengue, Oumar A. Niasse

Department of Physics, Cheick Anta Diop University (UCAD), Dakar, Senegal
Email: *badjisambou1995@gmail.com

How to cite this paper: Badji, I.S., Diaw, A., Diagne, M., Pilor, M., Mbengue, N. and Niasse, O.A. (2026) Structural and Electronic Properties of $Zn_{1-x}Mg_xO$ Alloys in WZ Phase with Hubbard Correction: Prospective Material for Optoelectronics Applications. *Crystal Structure Theory and Applications*, **14**, 1-13.
https://doi.org/10.4236/csta.2026.141001

Received: May 26, 2026
Accepted: July 26, 2026
Published: July 29, 2026

Abstract

In this work, we determined the structural and electronic properties of $Zn_{1-x}Mg_xO$ wurtzite minerals, where the Mg concentration, x, varies between 0 and 1. These properties were studied using the Quantum Espresso code, which is based on density functional theory (DFT) and pseudopotentials. All calculations were performed using the Generalized Gradient Approximation (GGA) with the exchange-correlation potential in the Perdew-Burke-Ernzerhof (PBE) formalism. The results show that the bandgap energies increase as the molar fractions of Mg increase. They also show that the valence band comprises three regions: a deep region resulting from the contribution of oxygen s states, an intermediate region resulting mainly from the contribution of zinc d states, and finally, a region corresponding to the valence band maximum and resulting essentially from oxygen p states. However, the conduction band consists mainly of zinc s states, magnesium s and p states, and oxygen p states.

Keywords

Wurtzite $Zn_{1-x}Mg_xO$, Structural and Electronic, PDOS

1. Introduction

Given their broad optical spectrum, ranging from near-visible UV to deep ultraviolet, oxides such as ZnO and MgO and their alloys have attracted considerable interest as materials for optoelectronic devices [1]-[7]. Furthermore, since the ionic radius of Mg^{2+} (0.57 Å) is similar to that of Zn^{2+} (0.60 Å), Zn can

be replaced by Mg to form the alloy [8]. Thanks to their tunable bandgaps (3.3 to 7.8), low growth temperatures (100˚C - 750˚C), and radiation resistance, $Zn_{1-x}Mg_xO$ wurtzite ternary compounds are ideal materials for the development of solar cells [9]. Wurtzite $Zn_{1-x}Mg_xO$ alloys can be synthesized for x values up to 0.66 [10].

Over the past few decades, numerous theoretical studies based on density functional theory, in which the LDA [11] and GGA [12] approximations were used, have been conducted to investigate the electronic and structural properties of ZnO. However, these studies did not yield satisfactory results in terms of accuracy, as they underestimate the bandgap values and incorrectly place the energy levels for the Zn-3d states. To correct the problem of bandgap underestimation, the authors of [13] and [14] proposed using the Hubbard correction, which yielded satisfactory results. It is in this context that, in this work, the structural and electronic properties of wurtzite $Zn_{1-x}Mg_xO$ (x = 0 to 1 in steps of 0.25) were calculated using DFT with the GGA + U functional. However, the x = 1 end corresponds to pure MgO in the wurtzite phase. This phase is treated here as a purely hypothetical reference obtained by calculation for extrapolation purposes.

2. Calculation Method

We then constructed a 2 × 2 × 1 wz-ZnO supercell using the VESTA software, and subsequently used magnesium atoms to replace zinc atoms for each configuration. For each configuration, there are several ways to replace the zinc atoms with magnesium atoms. However, we selected the one with the highest symmetry. Our calculations were performed using the QUANTUM ESPRESO code [15]. It is based on density functional theory, plane waves, and pseudopotentials. We used the generalized gradient approximation (GGA) with the exchange-correlation potential in the Perdew-Burke-Ernzerhof (PBE) formalism [12]. The interaction between ions and electron for all atoms is described by ultrasoft pseudopotentials obtained from the Quantum Espresso website. To strike a balance between computation time and accuracy, the cutoff energy of the plane wave is set to 400 eV. Integration by sampling special points on the Brillouin zone is performed using the Monkhorst-Pack method [16] with a 4 × 4 × 2 k-point grid. The Hubbard correction for Up-O and Ud-Zn is 6 and 10 eV, respectively [17]. The Mg $3s^2$, Zn $3d^{10}4s^2$, and O $2s^22p^4$ electrons are treated as valence states. In all calculations, the convergence thresholds and maximum force are 1 × 10^{-8} Ry and 0.001Ry/atom. The Brodyden-Fletcher-Goldfarb-Shanno (BFGS) minimization algorithm [18] was used for geometric and structural optimization.

The mathematical formalism of DFT was first developed by Kohn and Hohenberg and later by Kohn and Sham. In the Kohn-Sham formalism, the total energy is calculated as follows [11]:

$$E(n) = T_s(n) + \int v(r)n(r)\mathrm{d}r + \frac{1}{2}\iint \frac{n(r)n(r')}{|r-r'|}\mathrm{d}r\mathrm{d}r' + E_{xc}(n)$$

E_{xc} is known as the exchange-correlation energy.

The E_{xc} energy is expressed as follows [19]:

$$E_{xc}^{GGA}(n) = \int \varepsilon_{xc}^{GGA}\left[n(r), \nabla n(r)\right] d^3 r$$

The Hubbard-U correction is expressed by the following equation [20]:

$$E_{GGA+U}\left[n(r)\right] = E_{GGA}\left[n(r)\right] + E_U\left[n(r)\right] - E_{dc}$$

where E_{GGA} is the energy derived from the conventional GGA functional, E_U is the Hubbard energy, and E_{dc} is the double-counting correction energy.

3. Result and Discussion

3.1. Structural Properties

The lattice parameters of the equilibrium lattice for the unit cells of ZnO, MgO, and $Zn_{1-x}Mg_xO$ (where x ranges from 0.25 to 0.75 in steps of 0.25) were determined by relaxation calculations. For ZnO and MgO wurtzite, we obtained results of a = 3.2433 Å and c = 5.1960 Å, and a = 3.2577 Å and c = 5.0837 Å, respectively. Our values for ZnO are in agreement with theoretical [21]-[23] and experimental [14] [24] [25] results. However, the results found by Wang Zhi-Jun *et al.* (2009) [26] for a and b are slightly higher than ours. Regarding MgO, our results are consistent with those found theoretically or experimentally in the literature [24] [27]. However, the results reported by [22] [28] are higher than ours. For Zn1-xMgxO ($0.25 < x < 0.75$) wurtzite, our results were compared with those in [29] and are consistent. However, there is a slight difference between our values and those found in [22] [26] [28] [30]. Furthermore, we observe that the values of a increase with x and that those of c decrease as x increases. The variation of the lattice parameters a and c as a function of the Mg concentration x for $Zn_{1-x}Mg_xO$ in the wurtzite structure is shown in **Figure 1** and **Figure 2** below.

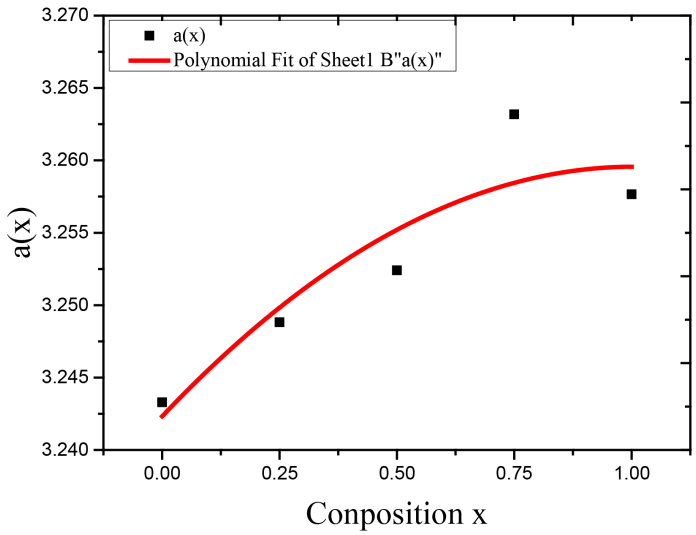

Figure 1. Variation of the mesh parameter a(x) as a function of the Mg content x.

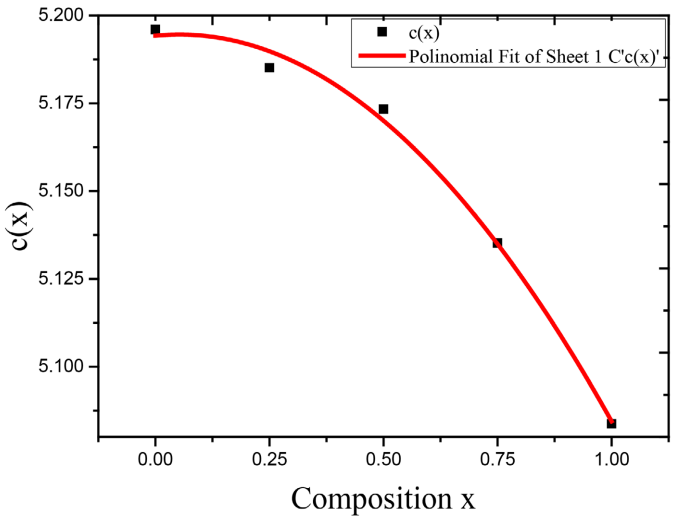

Figure 2. Variation of the mesh parameter c(x) as a function of the Mg content x.

We observe that this variation is nonlinear. This nonlinearity of a and c as a function of x means that the two lattice parameters deviate from Vegard's law, which states that the lattice parameters of ternary semiconductor alloys vary linearly with the molar fraction x (*i.e.*, (1 − x) for ZnO and x for MgO in our case). Furthermore, this observation is consistent with numerous experimental and theoretical results that have reported a deviation from Vegard's law in semiconductor alloys [22] [31] [32].

Therefore, the lattice parameters of $Zn_{1-x}Mg_xO$ can be written in the form [28]:

$$a_{(Zn_{1-x}Mg_xO)} = xa_{MgO} + (1-x)a_{ZnO} + bx(1-x)$$

$$c_{(Zn_{1-x}Mg_xO)} = xc_{MgO} + (1-x)c_{ZnO} + bx(1-x)$$

where the term b represents the linearity correction due to lattice distortion.

The polynomial fit of our data for a and c for the wurtzite $Zn_{1-x}Mg_xO$ yielded the following expressions:

$$a_{Zn_{1-x}Mg_xO} = 3.2423 + 0.0342x - 0.0170x^2$$

$$c_{Zn_{1-x}Mg_xO} = 5.1942 + 0.0130x - 0.1228x^2$$

Our results regarding the mesh parameters a and c are listed in **Table 1** below. Data from certain authors in the literature are also included for comparison purposes.

Table 1. Equilibrium lattice parameters of wurtzite $Zn_{1-x}Mg_xO$.

Mg composition x	a (Å)	c (Å)	c/a	u
0	3.2433[a], 3.28 [21], 3.28 [28], 3.28 [26], 3.24 [25]	5.1960[a], 5.24 [21], 5.28 [28], 5.29 [26], 5.20 [25]	1.6021[a], 1.59 [21], 1.61 [28], 1.61 [26], 1.60 [25]	0.379[a], 0.38 [21], 0.38 [21], 0.37 [27]
0.25	3.2488[a], 3.29 [30], 3.28 [28]	5.1851[a], 5.28 [30], 5.30 [28]	1.5960[a], 1.60 [30], 1.61 [28]	0.380[a]

Continued

0.5	3.2524[a], 3.30 [30], 3.28 [28]	5.1733[a], 5.27 [30], 5.29 [28]	1.5906[a], 1.59 [30], 1.60 [14]	0.381[a]
0.75	3.2631[a], 3.32 [30], 3.29 [14]	5.1351[a], 5.21 [30], 5.26 [14]	1.5736[a], 1.56 [30], 1.60 [28]	0384[a]
1	3.2576[a], 3.29 [28], 3.25 [24]	5.0837[a], 5.22 [28], 5.20 [24]	1.5605[a], 1.58 [28], 1.60 [24]	0.386[a], 0.388 [27]

[a]Our results.

3.2. Electronics Properties

3.2.1. Projected State Density

The properties of semiconductor materials are closely related to the electronic configuration of the atoms. Therefore, to study the distribution of electrons across the various orbitals, the PDOS (projected density of states) are calculated for the hexagonal wurtzite $Zn_{1-x}Mg_xO$.

The valence band consists precisely of three regions, as shown in **Figures 3-7** below.

The deepest region, or the region corresponding to the minimum of the valence band, consists mainly of the s states of the oxygen atom (O_s), with peaks observed between −15 and −17 eV regardless of the Mg concentration. The intermediate region, *i.e.*, the region between the minimum and maximum of the valence band, is essentially composed of the d states of the zinc atom (Zn_d), with peaks located between −8 and −11 eV for all configurations except for x = 1 (MgO). Furthermore, it is observed that an increase in Mg concentration leads to a narrowing of the Zn d-orbital band width. In the case of MgO, this region originates primarily from the p states of the oxygen atom.

The highest peak of the Zn d states for ZnO is located at approximately −9.5 eV, which is higher than the experimental results. Göpel *et al.* [33] and Powell *et al.* [34] performed UV photoemission and angle-resolved photoemission measurements, respectively, on vacuum-cleaved wurtzite ZnO, both of which placed the Zn d-band at approximately −7.5 eV. The X-ray photoemission results reported by Ruckh *et al.* [35] (−8.2 eV), Vesely *et al.* [36] (−8.5 eV), and Ley *et al.* [37] (−8.81 eV) are also higher but closer to our result than that of Powell *et al.* Finally, the shallowest region that is, the one closest to the Fermi level consists mainly of the p states of the oxygen atom. This observation was made for all configurations. In this region, peaks are observed around −1.25 to −6.9 eV. Regarding the conduction band, the main contributions come from the s states of the zinc atom for ZnO (x = 0), with peaks located between 1.5 and 13 eV. For the other configurations (x = 0.25, 0.5, 0.75), the contributions come mainly from the s states of zinc, the p and s states of magnesium, and the p states of oxygen. However, the s states of zinc and the p states of magnesium are clearly dominant. For MgO, the conduction band consists of the s and p states of magnesium and the s and p states of oxygen. However, the main contributions come from the s and p states of magnesium.

The following figures (**Figures 3-7**) show the PDOS of the $Zn_{1-x}Mg_xO$.

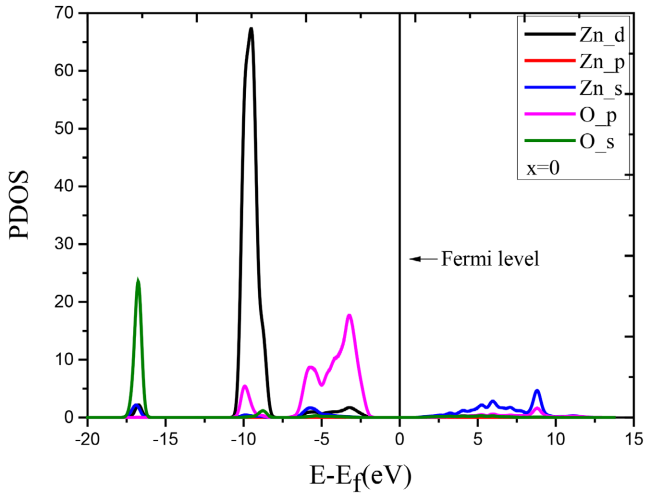

Figure 3. PDOS of the ZnO.

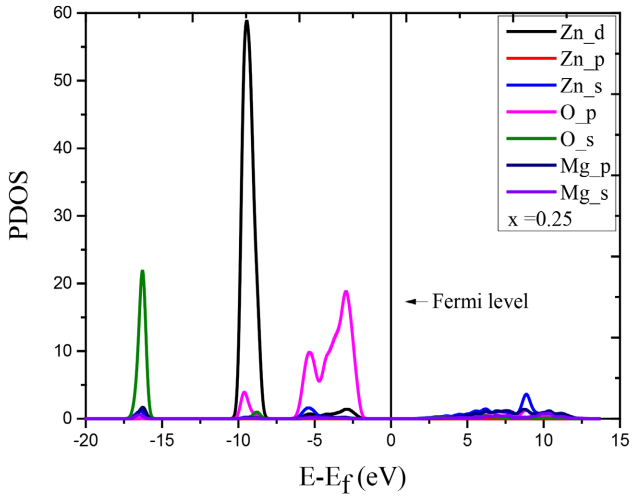

Figure 4. PDOS of the $Zn_{0.75}Mg_{0.25}O$.

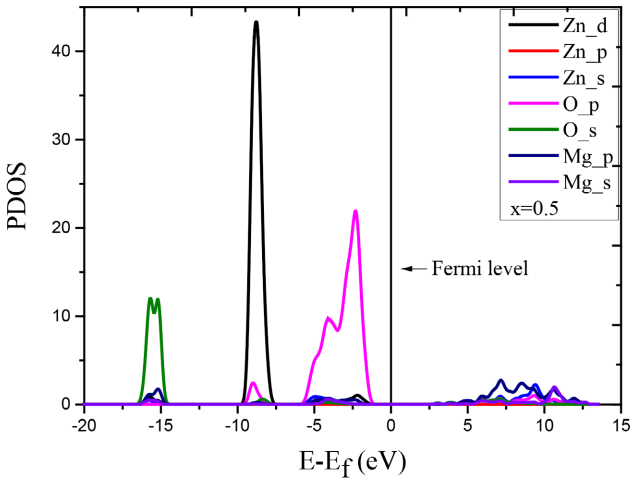

Figure 5. PDOS of the $Zn_{0.5}Mg_{0.5}O$.

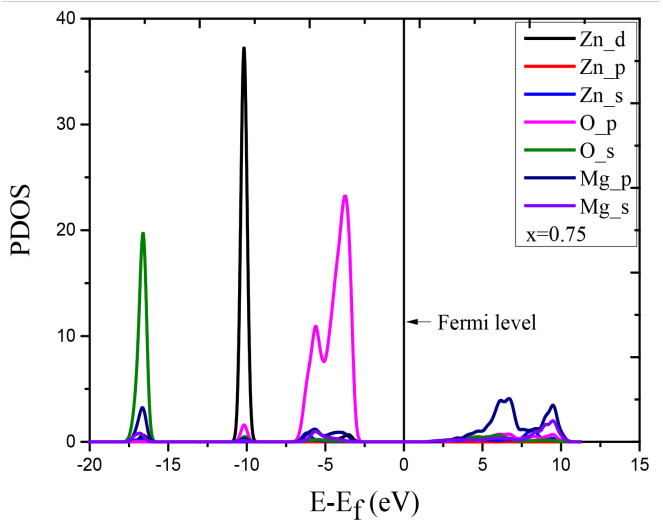

Figure 6. PDOS of the $Zn_{0.25}Mg_{0.75}O$.

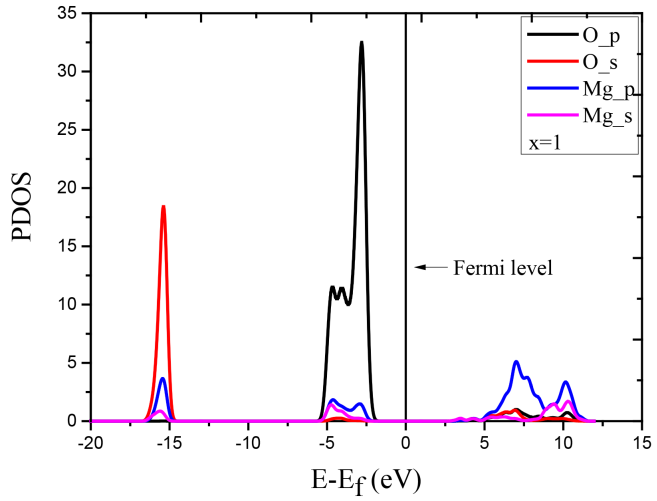

Figure 7. PDOS of the MgO.

3.2.2. Band Structure

In the literature, the bandgap of the ZnO wurtzite structure calculated by GGA ranges from 0.74 to 0.813 eV [17] [38], which is significantly underestimated compared to the experimental value. This underestimation is due to the fact that the GGA approximation is deficient and underestimates the binding energy of the Zn d states, leading to strong hybridization with the oxygen p states [23]. Thus, strong p-d coupling ultimately resulted in a smaller electronic energy gap than known experimental data. To address this issue, we used the PBE-GGA+U approach. Indeed, the Hubbard term (U) corrects the strong p-d hybridization between Zn and O, thereby shifting the Zn d states. ZnO and MgO (x = 0 and x = 1, respectively) are characterized by a direct bandgap located at the center of the Brillouin zone at the Γ point, where the bandgap values Eg are 3.4 eV and 5.5 eV, respectively. Our result for ZnO is in agreement with the experimental value (Eg = 3.44 eV [35]).

However, the value found for MgO (5.5 eV) is larger than the theoretically obtained value (5.328 eV) and smaller than the experimentally measured value (7.67 eV) reported by Taib *et al*. [39] and Y. Z. Zhu *et al*. [40], respectively.

The band structures for $0 < x < 1$, respectively, are shown in the figures (**Figures 8-12**) below.

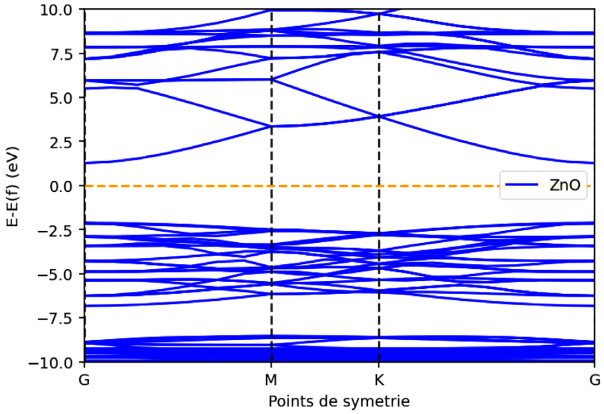

Figure 8. Band structure of ZnO.

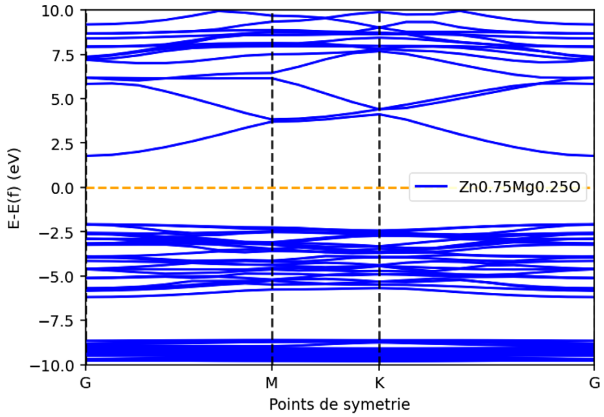

Figure 9. Band structure of $Zn_{0.75}Mg_{0.25}O$.

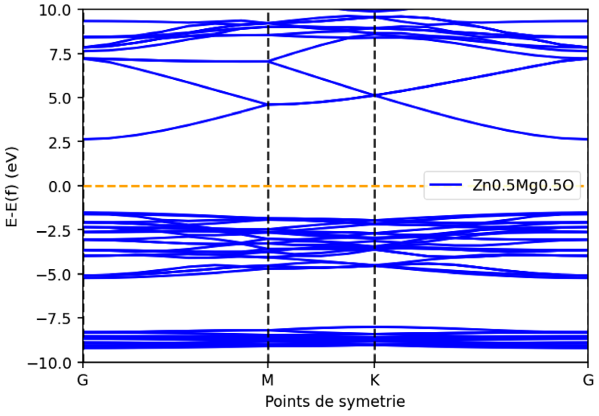

Figure 10. Band structure of $Zn_{0.5}Mg_{0.5}O$.

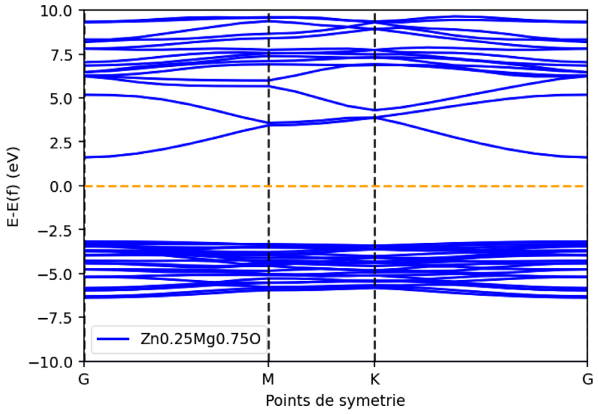

Figure 11. Band structure of $Zn_{0.25}Mg_{0.75}O$.

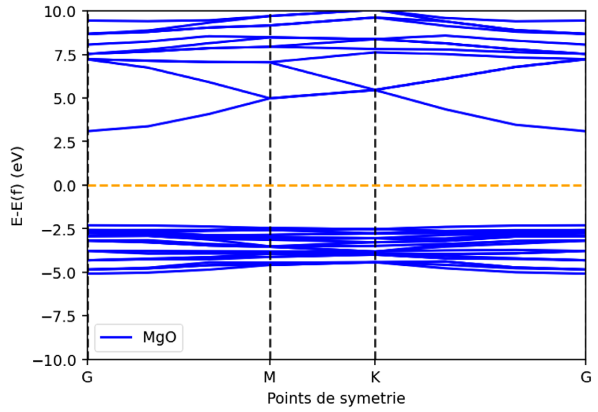

Figure 12. Band structure of MgO.

Our results are presented in Table 2 below. There are differences between our results and those found in the literature, which are shown in the table. This difference may be due to differences in the structural model or in the arrangement of the constituent alloys. It is important to note that there are no points of intersection between the Fermi level and the energy bands for any of our configurations. Consequently, $Zn_{1-x}Mg_xO$ (x = 0, 0.25, 0.50, 0.75, and 1) in the hexagonal wurtzite structure can be considered a semiconductor material. In addition, we observe that the band energy of the $Zn_{1-x}Mg_xO$ ternary alloys increases as the Mg concentration (x) increases. Our results and some findings from the literature are summarized in Table 2 below.

Table 2. Gap band values for wurtzite $Zn_{1-x}Mg_xO$.

Mg composition x	Band gap (eV)	Other results
0	3.4	3.44 [14], 3.44 [40]
0.25	4.0	3.19 [29]
0.5	4.30	3.71 [29]
0.75	4.7	4.36 [29]
1	5.5	5.328 [40], 7.67 [40]

The polynomial fit of our data for the band gap of wurtzite $Zn_{1-x}Mg_xO$ yielded the following expression:

$$E_g(x) = 3.4714 + 1.3885x + 0.5714x^2$$

In our calculations, we found a Bowing parameter b = 0.5714, which differs from the value found by A. Djelal *et al.* [22] and F.Z. Aouacheria *et al.* [28].

The variation of the band gap (Γ - Γ) as a function of Mg concentration, x, for hexagonal wurtzite $Zn_{1-x}Mg_xO$ is shown in **Figure 13** below.

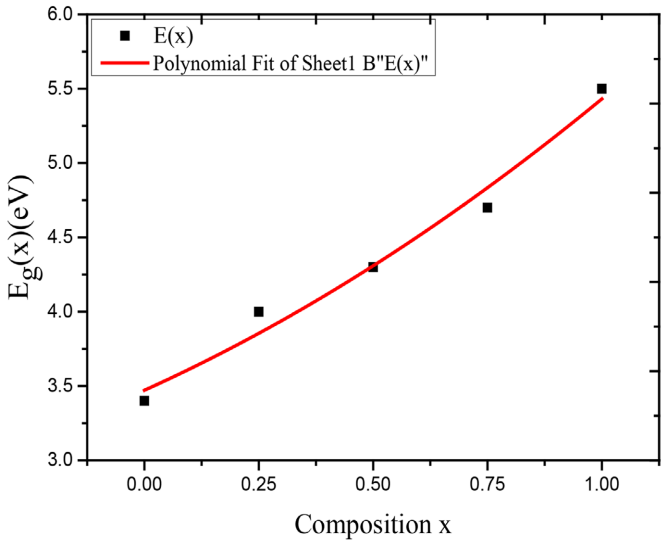

Figure 13. Change in the band gap as a function of the Mg concentration x.

4. Conclusions

In this study, we presented a comprehensive theoretical analysis of the structural and electronic properties of $Zn_{1-x}Mg_xO$ alloys, which were calculated using DFT + U. We observed a nonlinear behavior for both lattice parameters a and c, indicating a violation of Vegard's empirical law.

Second, it is well known that the experimental bandgap is underestimated by conventional DFT. The use of the Hubbard correction $U_{d\text{-}Zn}$ and $U_{p\text{-}O}$ allowed for the correct reproduction of the band gap for ZnO, but not for MgO. Furthermore, the valence band generally consists of three main regions, and the conduction band was found to be dominated by the Zn_s, Mg_p, and Mg_s states.

Conflicts of Interest

The authors declare no conflicts of interest regarding the publication of this paper.

References

[1] Long, H., Fang, G., Li, S., Mo, X., Wang, H., Huang, H., *et al.* (2011) A ZnO/ZnMgO Multiple-Quantum-Well Ultraviolet Random Laser Diode. *IEEE Electron Device Letters*, **32**, 54-56. https://doi.org/10.1109/led.2010.2089424

[2] Yang, H.S., Han, S.Y., Heo, Y.W., Baik, K.H., Norton, D.P., Pearton, S.J., *et al*. (2005) Fabrication of Hybrid *n*-ZnMgO/*n*-ZnO/*p*-AlGaN/*p*-GaN Light-Emitting Diodes. *Japanese Journal of Applied Physics*, **44**, 7296-7300. https://doi.org/10.1143/jjap.44.7296

[3] Alam, M.J., Murkute, P., Sushama, S., Ghadi, H., Paul, S., Mondal, S., *et al*. (2020) Improving Optical Properties and Controlling Defect-Bound States in ZnMgO Thin Films through Ultraviolet-Ozone Annealing. *Thin Solid Films*, **708**, Article 138112.

[4] Ghadi, H., Murkute, P., Ghosh, A., Dwivedi, S.M.M.D., Mondal, A. and Chakrabarti, S. (2018) Ultrasensitive Zinc Magnesium Oxide Nanorods Based Micro-Sensor Platform for UV Detection and Light Trapping. *Sensors and Actuators A*: *Physical*, **278**, 127-139. https://doi.org/10.1016/j.sna.2018.05.028

[5] Zheng, Q., Huang, F., Huang, J., Hu, Q., Chen, D. and Ding, K. (2012) High-Responsivity Solar-Blind Photodetector Based on $Mg_{0.46}Zn_{0.54}O$ Thin Film. *IEEE Electron Device Letters*, **33**, 1033-1035. https://doi.org/10.1109/led.2012.2196675

[6] Fortunato, E., Barquinha, P. and Martins, R. (2012) Cheminform Abstract: Oxide Semiconductor Thin-Film Transistors: A Review of Recent Advances. *ChemInform*, **43**, No. 34. https://doi.org/10.1002/chin.201234192

[7] Li, J.-Y., Chang, S.-P., Hsu, M.-H. and Chang, S.-J. (2018) Photo-Electrical Properties of MgZnO Thin-Film Transistors with High-*K* Dielectrics. *IEEE Photonics Technology Letters*, **30**, 59-62.

[8] Sonawane, B.K., Bhole, M.P. and Patil, D.S. (2009) Structural, Optical and Electrical Properties of Post Annealed Mg Doped ZnO Films for Optoelectronics Applications. *Optical and Quantum Electronics*, **41**, 17-26. https://doi.org/10.1007/s11082-009-9317-y

[9] Ren, S., Wang, H., Li, Y., Li, H., *et al*., (2018) Rapid Thermal Annealing on ZnMgO Window Layer for Improved Performance of CdTe Solar Cells. *Solar Energy Materials and Solar Cells*, **187**, 97-103.

[10] Trinkler, L., Aulika, I., Krieke, G., Nilova, D., *et al*. (2022) Characterization of Wurtzite $Zn_{1-x}Mg_xO$ Epilayers Grown on $ScAlMgO_4$ Substrate by Methods of Optical Spectroscopy. *Journal of Alloys and Compounds*, **912**, Article 165178.

[11] Kohn, W. and Sham, L.J. (1965) Self-Consistent Equations Including Exchange and Correlation Effects. *Physical Review*, **140**, A1133-A1138. https://doi.org/10.1103/physrev.140.a1133

[12] Perdew, J.P., Burke, K. and Ernzerhof, M. (1996) Generalized Gradient Approximation Made Simple. *Physical Review Letters*, **77**, 3865-3868. https://doi.org/10.1103/physrevlett.77.3865

[13] Walsh, A., Da Silva, J.L.F. and Wei, S. (2008) Theoretical Description of Carrier Mediated Magnetism in Cobalt Doped ZnO. *Physical Review Letters*, **100**, Article 256401. https://doi.org/10.1103/physrevlett.100.256401

[14] Ma, X., Wu, Y., Lv, Y. and Zhu, Y. (2013) Correlation Effects on Lattice Relaxation and Electronic Structure of ZnO within the GGA+U Formalism. *The Journal of Physical Chemistry C*, **117**, 26029-26039. https://doi.org/10.1021/jp407281x

[15] Giannozzi, P., Baroni, S., Bonini, N., Calandra, M., Car, R., Cavazzoni, C., *et al*. (2009) Quantum Espresso: A Modular and Open-Source Software Project for Quantum Simulations of Materials. *Journal of Physics*: *Condensed Matter*, **21**, Article 395502. https://doi.org/10.1088/0953-8984/21/39/395502

[16] Monkhorst, H.J. and Pack, J.D. (1976) Special Points for Brillouin-Zone Integrations. *Physical Review B*, **13**, 5188-5192. https://doi.org/10.1103/physrevb.13.5188

[17] Harun, K., Salleh, N.A., Deghfel, B., Yaakob, M.K. and Mohamad, A.A. (2019) DFT+U Calculations for Electronic, Structural, and Optical Properties of ZnO Wurtzite Structure: A Review. *Results in Physics*, **16**, Article 102829. https://doi.org/10.1016/j.rinp.2019.102829

[18] Fischer, T.H. and Almlof, J. (1992) General Methods for Geometry and Wave Function Optimization. *The Journal of Physical Chemistry*, **96**, 9768-9774. https://doi.org/10.1021/j100203a036

[19] Haas, P., Tran, F., Blaha, P., Schwarz, K. and Laskowski, R. (2009) Insight into the Performance of GGA Functionals for Solid-State Calculations. *Physical Review B*, **80**, Article 195109. https://doi.org/10.1103/physrevb.80.195109

[20] Cococcioni, M. and de Gironcoli, S. (2005) Linear Response Approach to the Calculation of the Effective Interaction Parameters in the LDA+U Method. *Physical Review B*, **71**, Article 035105. https://doi.org/10.1103/physrevb.71.035105

[21] Özgür, Ü., Alivov, Y.I., Liu, C., Teke, A., Reshchikov, M.A., Doğan, S., *et al*. (2005) A Comprehensive Review of ZnO Materials and Devices. *Journal of Applied Physics*, **98**, Article 041301. https://doi.org/10.1063/1.1992666

[22] Djelal, A., Chaibi, K., Tari, N., Zitouni, K. and Kadri, A. (2017) Ab-Initio DFT-FP-LAPW/TB-mBJ/LDA-GGA Investigation of Structural and Electronic Properties of $Mg_xZn_{1-x}O$ Alloys in Würtzite, Rocksalt and Zinc-Blende Phases. *Superlattices and Microstructures*, **109**, 81-98. https://doi.org/10.1016/j.spmi.2017.04.041

[23] Mohamad, A.A., Hassan, M.S., Yaakob, M.K., *et al*. (2015) First-Principles Calculation on Electronic Properties of Zinc Oxide by Zinc-Air System. *Journal of King Saud University-Engineering Sciences*, **29**, 278-283.

[24] Toporkov, M., Demchenko, D.O., Zolnai, Z., Volk, J., Avrutin, V., Morkoç, H., *et al*. (2016) Lattice Parameters and Electronic Structure of BeMgZnO Quaternary Solid Solutions: Experiment and Theory. *Journal of Applied Physics*, **119**, Article 095311. https://doi.org/10.1063/1.4942835

[25] Karzel, H., Potzel, W., Köfferlein, M., Schiessl, W., Steiner, M., Hiller, U., *et al*. (1996) Lattice Dynamics and Hyperfine Interactions in ZnO and ZnSe at High External Pressures. *Physical Review B*, **53**, 11425-11438. https://doi.org/10.1103/physrevb.53.11425

[26] Wang, Z.-J., Li, S.-C., Wang, L.-Y. and Liu, Z. (2009) First-Principles Study of Structural and Corrected Band Properties of Wurtzite $Zn_{1-X}Cd_xO$ and $Zn_{1-X}Mg_xO$ Systems. *Chinese Physics B*, **18**, 2992-2997. https://doi.org/10.1088/1674-1056/18/7/062

[27] Shimada, K., Takahashi, N., Nakagawa, Y., Hiramatsu, T. and Kato, H. (2013) Nonlinear Characteristics of Structural Properties and Spontaneous Polarization in Wurtzite $Mg_xZn_{1-x}O$: A First-Principles Study. *Physical Review B*, **88**, Article 075203. https://doi.org/10.1103/physrevb.88.075203

[28] Aouacheria, F.Z., Telia, A. and Meziani, A. (2020) Investigation on Structural and Electronic Properties of $Zn_{1-x}Mg_xO$ in Wurtzite Phase Using First Principal Calculations. 2020 *IEEE International Conference on Design & Test of Integrated Micro & Nano-Systems* (*DTS*), Hammamet, 7-10 June 2020, 1-5. https://doi.org/10.1109/dts48731.2020.9196142

[29] Lin, Y., Piskunov, S., Trinkler, L., Ming-Chi Chou, M. and Chang, L. (2022) Electronic and Optical Properties of Rocksalt $Mg_xZn_{1-x}O$ and Wurtzite $Zn_{1-x}Mg_xO$ with Varied Concentrations of Magnesium and Zinc. *Materials*, **15**, Article 7689. https://doi.org/10.3390/ma15217689

[30] Gao, J., Zhao, G.J., Liang, X.X. and Song, T.L. (2015) First-Principles Study of Struc-

tural Properties of $Mg_xZn_{1-x}O$ Ternary Alloys. *Journal of Physics*: *Conference Series*, **574**, Article 012169. https://doi.org/10.1088/1742-6596/574/1/012169

[31] Dismukes, J.P., Ekstrom, L. and Paff, R.J. (1964) Lattice Parameter and Density in Germanium-Silicon Alloys. *The Journal of Physical Chemistry*, **68**, 3021-3027. https://doi.org/10.1021/j100792a049

[32] Charifi, Z. and Bouarissa, N. (1997) The Effect of the Violation of Vegard's Law on the Optical Bowing in $Si_{1-x}Ge_x$ Alloys. *Physics Letters A*, **234**, 493-497. https://doi.org/10.1016/s0375-9601(97)00575-6

[33] Göpel, W., Pollmann, J., Ivanov, I. and Reihl, B. (1982) Angle-Resolved Photoemission from Polar and Nonpolar Zinc Oxide Surfaces. *Physical Review B*, **26**, 3144-3150. https://doi.org/10.1103/physrevb.26.3144

[34] Powell, R.A., Spicer, W.E. and McMenamin, J.C. (1971) Location of the Zn 3d States in ZnO. *Physical Review Letters*, **27**, 97-100. https://doi.org/10.1103/physrevlett.27.97

[35] Ruckh, M., Schmid, D. and Schock, H.W. (1994) Photoemission Studies of the ZnO/CdS Interface. *Journal of Applied Physics*, **76**, 5945-5948. https://doi.org/10.1063/1.358417

[36] Vesely, C.J., Hengehold, R.L. and Langer, D.W. (1972) UV Photoemission Measurements of the Upper *d* Levels in the IIB-VIA Compounds. *Physical Review B*, **5**, 2296-2301. https://doi.org/10.1103/physrevb.5.2296

[37] Ley, L., Pollak, R.A., McFeely, F.R., Kowalczyk, S.P. and Shirley, D.A. (1974) Total Valence-Band Densities of States of III-V and II-VI Compounds from X-Ray Photoemission Spectroscopy. *Physical Review B*, **9**, 600-621. https://doi.org/10.1103/physrevb.9.600

[38] Jafarova, V.N. and Orudzhev, G.S. (2021) Structural and Electronic Properties of ZnO: A First-Principles Density-Functional Theory Study within LDA(GGA) and LDA(GGA)+U Methods. *Solid State Communications*, **99**, Article 065927.

[39] Taib, M.F.M., Mustaffa, D.T., Hussin, N.H., Samat, M.H., Ali, A.M.M., Hassan, O.H., *et al*. (2019) First Principles Study on Zn Doped MgO Using Hubbard U Correction. *Materials Research Express*, **6**, Article ID: 094012. https://doi.org/10.1088/2053-1591/ab1200

[40] Zhu, Y.Z., Chen, G.D., Ye, H., Walsh, A., Moon, C.Y. and Wei, S. (2008) Electronic Structure and Phase Stability of MgO, ZnO, CdO, and Related Ternary Alloys. *Physical Review B*, **77**, Article 245209. https://doi.org/10.1103/physrevb.77.245209